PPPL-1952

DIAGNOSTICS FOR HOT PLASMAS USING HYDROGEN NEUTRAL BEAMS

By

R.J. Goldston

DECEMBER 1982

PLASMA PHYSICS LABORATORY

PRINCETON UNIVERSITY

PRINCETON, NEW JERSEY

PREPARED FOR THE U.S. DEPARTMENT OF ENERGY, UNDER CONTRACT DE-AC02-76-CHO-3073.

NOTICE

Printed in the United States of America.

Available from:

National Technical Information Service
U. S. Department of Commerce
5285 Port Royal Road
Springfield, Virginia 22151

Price: Printed Copy $ * : Microfische $3.50

*PAGES	NTIS Selling Price
1-25	$5.00
26-50	$6.50
51-75	$8.00
76-100	$9.50
101-125	$11.00
126-150	$12.50
151-175	$14.00
176-200	$15.50
201-225	$17.00
226-250	$18.50
251-275	$20.00
276-300	$21.50
301-325	$23.00
326-350	$24.50
351-375	$26.00
376-400	$27.50
401-425	$29.00
426-450	$30.50
451-475	$32.00
476-500	$33.50
500-525	$35.00
526-550	$36.50
551-575	$38.00
576-600	$39.50

For documents over 600 pages, add $1.50 for each additional 25 page increment.

PPPL--1952

DIAGNOSTICS FOR HOT PLASMAS USING HYDROGEN NEUTRAL BEAMS

DE83 003904

Dr. Robert J. Goldston

Princeton University, Plasma Physics Laboratory

Princeton, New Jersey 08544

ABSTRACT

Beams of neutral hydrogen atoms have found a number of uses in the diagnosis of hot plasmas. In the most straightforward application, neutral beams have been used to determine plasma line density, based on simple attenuation measurements. This technique has been applied most intensively recently to the study of beam-injected mirror plasmas. Neutral beams have also now been used in a number of tokamaks to supply a local increase of the neutral atom "target" density for charge exchange. By directing a time-modulated neutral beam across the sight-line of a charge-exchange analyzer, and measuring the modulated neutral particle efflux from the plasma, local measurements of the ion energy distribution function can be made. If a modulated diagnostic neutral beam is directed across the sight-line of an ultra-violet spectrometer, one can also make measurements of the local densities and possibly velocity distributions of fully stripped impurities. The fast hydrogen neutrals charge exchange with fully stripped impurities in the plasma, leaving the impurities in excited hydrogen-like states. In their prompt radiative decay the impurity ions emit characteristic UV lines, which can be detected easily.

In more exotic applications, one makes use of the circulating ion beam deposited in the plasma by tangential injection of a diagnostic neutral beam. Using a charge-exchange analyzer to measure the angular spectrum of the

ions, the pitch-angle scattering rate, and therefore Z_{eff}. can be determined. By studying the orbits of these ions, one can measure q(r). Finally the spatial motion of the circulating ions due to MHD and other activity can be studied by examining their slowing-down spectrum.

BEAM ATTENUATION MEASUREMENTS

One of the earliest diagnostic applications of particle beams for magnetically confined plasmas was to measure the attenuation of a neutral beam as it passed through the plasma column /1/. Given knowledge of the plasma composition and of the relevant cross sections, this technique can be used to measure the plasma line density:

$$nl = \frac{1}{\sigma_{tot}} \ell n(I/I_o) \ , \tag{1}$$

where I_o is the beam current detected in the absence of plasma attenuation, and I is the current measured during the plasma discharge. σ_{tot} is the total effective cross section for ionization of the neutral beam by charge exchange, ion impact ionization, and electron impact ionization.

$$n\sigma_{tot}v = \sum_j n_j \left(\langle \sigma v \rangle_{cx} + \langle \sigma v \rangle_{iii} \right)_j + n_e \langle \sigma v \rangle_{eii} \ , \tag{2}$$

where the sum over j represents a sum over ion species within the plasma. A compilation of reaction rates for collisions of hydrogenic neutrals with hydrogenic ions and electrons is available in /2/. A reasonably accurate scaling rule for computing the total electron loss cross sections for non-hydrogenic target ions is given in /3/.

$$\left(\sigma_{cx} + \sigma_{ii}\right)_j \simeq 4.6 Z_j \times 10^{-16} \times \left\{ Q\left[1 - \exp(-1/Q) \right] \right\} \tag{3}$$

where $Q = 32 Z_j A/E$, and E/A is the neutral beam energy, in keV/AMU.

Only a rather modest hydrogen neutral beam of typically a few tens of milliamperes is required for this application, although close attention must

be paid to sources of beam attenuation other than the plasma itself. Neutral particle analyzers, similar to those employed for ion temperature measurement, are often used to detect the beam.

Beam attenuation measurements of plasma density have largely been supplanted by microwave and laser interferometry techniques, with which uncertainties about plasma composition and attenuation cross sections do not play a role. Interferometers, however, require a relatively quiet plasma in order to provide countable "fringes" /4/, since the density measurement at any one time requires knowledge of the full evolution of the interference pattern up to that time. By contrast, beam attenuation measurements are rather immune to plasma noise. In the 2XIIB device the attenuation of a 20 keV neutral deuterium beam, similar to the main heating and fueling beams, has been used to measure the plasma density /5/. Because of the high current density employed, an array of simple secondary emission detectors allowed the measurement of the full axial and radial density profiles. Some unfolding was required in order to take into account the three energy species generated by the neutral beam and the ion energy distribution within the plasma.

While beam attenuation measurements are not widely used in quiescent plasmas, due in part to their sensitivity to plasma ion composition, this apparent disadvantage can be turned to an advantage by making the attenuation measurements in conjunction with an independent measurement of electron density. This technique can be used to determine the fraction of impurities contained in the plasma, particularly if spectroscopic or other measurements can give the dominant impurity species present /6/.

In this case, however, one is trying to measure the difference between $n_j (\langle\sigma v\rangle_{cx} + \langle\sigma v\rangle_{iii})_j$ and $Z_j n_h (\sigma v\rangle_{cx} + \langle\sigma v\rangle_{iii})_h$. Equation (3) shows that in the energy range easily available to hydrogen neutral beam technology (E = 5 +

100 keV) and for impurity charge states of interest ($Z_j \gtrsim 6$), the reaction rates for impurities are fairly close to Z times the reaction rate for hydrogenic ions. Since each impurity ion "replaces" Z_j hydrogenic ions, by quasi-neutrality, this makes the measurement difficult. In practice, however, deviations of specific cross sections, both as measured and as calculated, from Eq. (3) make the problem somewhat easier.

ACTIVE CHARGE EXCHANGE

Even so called "fully ionized" high temperature fusion plasmas are permeated by a low backround density of neutral hydrogen atoms. This is because, over most of the energy range of interest, the reaction rate for charge exchange between hydrogen atoms and hydrogen ions is much greater than the reaction rate for electron impact ionization or for ion impact ionization. Relatively slow neutral atoms are created at the plasma surface either by dissociation of feed gas and wall-desorbed hydrogen giving ~ 3 eV atomic neutrals, or by reflection of escaping plasma ions from the limiter surface, giving neutrals in the energy range characteristic of the edge plasma ion temperature. These neutrals themselves typically have relatively short mean free paths against electron impact ionization. By charge exchanging with more energetic ions within the plasma, however, they give rise to "generations" of hotter neutrals, able to penetrate quite deeply into the discharge /7/. This process is shown schematically in Fig. 1.

While neutral atoms within an ionized plasma give rise to an energy loss channel, they also make possible a reasonably simple technique for measuring the energy distribution of the magnetically confined ions. Even when the mean free path of a neutral atom in the core of the plasma is small compared to the plasma radius, some of the neutrals generated by charge exchange in the hot

central region are able to escape from the discharge. The mean free path with respect to the sum of charge exchange and impact ionization increases approximately in proportion to the neutral energy. As a result, at very high line integral electron densities, particles generated by charge exchange from the energetic tail of the central ion distribution function are most likely to escape from the plasma. The emerging particles are detected with a neutral particle analyzer (NPA), which typically consists of a gas stripping cell to convert neutral atoms to ions, an electrostatic (and in some cases magnetic) ion spectrometer to permit energy (and in some cases mass) resolution of the particles, and finally, an array of particle detectors typically based on some form of electron multiplier.

From the analyzer calibration as a function of energy, and knowing the acceptance angle, the measured raw count rates can be converted to a flux at the front aperture, F, measured in units of particles/(sec • cm^2 • steradian/4π • eV).

In order to work back to the ion energy distribution, the flux at the analyzer is divided by the energy dependent charge exchange rate coefficient $\sigma_{cx}v$, and by the square root of the particle energy. The quantity that is usually plotted as the "charge exchange spectrum" is actually

$$f_{cx} = \frac{F(E)}{\sigma_{cx}v \cdot \sqrt{E}} \quad . \tag{4}$$

For a Maxwellian ion distribution function, and ignoring attenuation of escaping neutrals, the spectrum should be simply of the form $f_{cx} \propto \exp(-E/T_i)$. Putting the spectrum on a semi-log plot one should obtain a straight line whose slope reflects the ion temperature. In most situations, however, the plasma does not have a unique ion temperature, but rather a

temperature profile peaked at the plasma center and falling to a low value at the edge. This problem is further complicated by the fact that the neutral density, and so the charge exchange production rate, is strongly peaked near the plasma surface, as discussed above. The result is that the charge exchange spectrum measured by this "passive" technique is curved at low energies, but becomes a straight line on a semi-log plot above $E \sim 2\text{-}3T_i(0)$ (Fig. 2a). This is because the contribution to the spectrum from the cold edge region of the plasma becomes negligibly small at high energies, and so the neutral particle analyzer eventually measures only the central distribution function.

If one has confidence that the central ion energy distribution is Maxwellian with a single temperature out to high energies, the ion temperature can then be measured, in moderate density plasmas, by fitting the spectrum with a simple exponential in the region of $\sim$ 3 to 10 T_i. In general, one finds that the small underestimate in $T_i(0)$ that results from the contributions to the charge exchange flux due to regions away from the plasma center is partially compensated by the overestimate in $T_i(0)$ associated with the inability of low energy neutrals to escape from the plasma center and reach the NPA. The result is that at moderate $n_e \cdot 1/T_i \sim 10^{15}$ cm^{-2} keV^{-1} the slope of the high energy region tends to give a surprisingly accurate measure of $T_i(0)$. In very high density plasmas, however, one has to measure at extremely high values of E/T_i in order to find a straight line region of the spectrum, and the count rate at these energies is unacceptably low. In this case, modeling of the process by which the spectrum is produced becomes necessary in order to deduce the central ion temperature.

Given confidence in the Maxwellian nature of the ion energy distribution, and given confidence in a calculation of the neutral density profile, much

information can be gleaned from the details of the charge exchange energy spectrum. In principle enough information is available to permit a reconstruction of the full ion temperature profile. In practice, however, the ion temperature profile is often assumed to be of the form

$$T_i(r) = T_i(0) \left[1 - (r/a)^2 \right]^{\alpha} \quad . \tag{5}$$

$T_i(0)$ and α are then determined together from the shape of the charge exchange spectrum /8/. This requires modeling the neutral transport within the plasma and the transport of fast neutrals to the NPA, and then performing a least squares fit to the measured spectrum, varying $T_i(0)$ and α. The absolute magnitude of the calculated neutral density profile can also be determined from the intensity of the measured neutral particle flux.

This technique of coupling charge exchange measurements with extensive numerical modeling has the advantage that it makes maximal use of the available information. It has the disadvantage that it relies heavily on uncertain assumptions about $n_o(r)$ and $f_i(E)$. Poloidal and toroidal asymmetries in the neutral source and non-Maxwellian features in the ion distribution function cannot easily be included. A much superior alternative approach is to make a direct charge exchange measurement of the local ion energy distribution /9,10,11,12/. In this technique a diagnostic neutral beam is used to dope the plasma locally with a time-modulated neutral density. The doping gives rise to a modulation in the neutral flux at the analyzer, resulting from the increment in charge exchange production at the point in the plasma along the detector sight-line where it crosses the doping beam path. Figure 3 shows the increase in neutral particle signal from an ohmically heated PDX plasma, due to a 15 msec long doping beam pulse. By normalizing

out the energy dependence of both the charge exchange production rate and of the attenuation probability of the emerging neutrals, the local ion energy distribution function can be deduced from the measured modulation in neutral flux. Figure 2b shows the result of such an analysis for the same discharge in which the passive spectrum shown in Fig. 2a was measured.

An interesting problem arises when one looks into the details of this sort of measurement. There are actually two sources of increased flux due to the doping beam. The first source is simple charge exchange between the energetic beam neutrals and the plasma ions. This is, of course, relatively simple to calculate on the basis of known cross sections /2/. The experimental difficulties are that one needs to obtain accurate knowledge of the beam profile shape, species mix (E_{inj}, $E_{inj}/2$, $E_{inj}/3$), absolute power to the torus, and degree of penetration. The second process, however, presents a more fundamental problem. When the beam neutrals undergo charge exchange with the plasma ions, they generate thermal neutrals, most of which typically do not immediately escape from the plasma. Through the multi-generation charge exchange process a "halo" of these thermal plasma neutrals is created around the primary beam neutrals. This halo is broader than the beam itself, since the multiple charge exchange events allow the neutrals to diffuse. The halo is also essentially perfectly time correlated with the beam modulation, because electron ionization times, which set an upper limit on the halo lifetime, are in the microsecond range for neutral hydrogen in typical high temperature plasmas.

Figure 4 shows the geometrical layout for the thermal charge exchange diagnostic on TFTR /13/. Note that the beam and detector sight-lines cross at 90°. This means that the relative energy between an injected beam neutral at $E = E_{inj}$ keV/AMU and a plasma ion at $E = E_{det}$ keV/AMU is simply $E_{rel} = E_{inj} +$

E_{det}. For adequate beam penetration in TFTR, one will require $E_{inj} \sim 40$ keV/AMU. If $T_i(0)$ attains values above 10 keV, as anticipated, then it will be desirable to measure the ion distribution up to energies at least as high as 50 keV. This puts E_{rel} at 90 keV/AMU for a hydrogen target plasma, in a range where the charge exchange cross section has fallen to a very low value. The 40 keV/AMU neutral beam, however, generates a substantial charge exchange halo. The line density of the halo along the detector sight-line is comparable to the beam neutral line density, and the halo neutrals have a temperature close to the local ion temperature. The halo therefore becomes the dominant source of enhanced neutral target for charge exchange in this situation (Fig. 5). To make accurate calculations of the beam halo density profile requires the use of a 3-D Monte Carlo neutral transport code /14/, although a 1-D diffusive model should give a reasonable estimate.

CHARGE EXCHANGE RECOMBINATION

One of the persistent problems in the use of spectroscopic techniques to assess the impurity content of hot plasmas is that fully ionized impurities do not emit line radiation, and so they are not easily detectable. Fully stripped ions contribute to free-bound recombination radiation, and to free-free bremstrahlung radiation. Jumps in the continuum soft X-ray radiation at $E = 13.6\ Z^2$ (eV) are caused by recombination edges associated with radiative recombination of zero-energy electrons. In principle these jumps can be used to determine the density profile of different species of fully-stripped impurities. In practice, however, the recombination edges of typical low-Z impurities such as carbon and oxygen are in an inconvenient region of the extreme soft X-ray spectrum, and accurate measurements are difficult to make. The continuum bremstrahlung radiation, particularly in the visible

region of the spectrum where recombination is unimportant, has recently been used to measure Z_{eff} (r,t) /15/. These measurements, however, do not permit discrimination between the different impurities which contribute to Z_{eff}.

A hydrogen neutral beam, in traversing an impure plasma, undergoes charge exchange reactions with the impurities /16,17,18,19,20/, as well as charge exchange with hydrogen ions, and impact ionization collisions with bulk ions, electrons, and impurities /2,3/. In particular, the reaction

$$H^0 + X^{+z} \rightarrow H^+ + X^{+z-1*}$$

can be especially useful for plasma diagnostics when z is equal to the atomic number, Z, of impurity X. In this reaction, fully ionized impurities are converted to hydrogen-like ions in excited states. For typical hydrogen neutral beam energies of 25-100 keV/AMU, the charge exchange process tends to predominately populate principal quantum numbers around $n = Z^{3/4}$ /17,20/. These states have lifetimes in the nanosecond range, so that the excited hydrogen-like ions decay to their ground states before they move significantly from the location of the collision. Thus, by observing the prompt ultraviolet radiation which is produced along the path of a neutral beam within a plasma, one can measure the local density of fully ionized impurities /21,22,23/. Calculations of the relevant recombination cross sections are available over a range of energies, in some cases including also the n and ℓ state distributions produced by the reactions. Transition probabilities are easily calculated for hydrogen-like ions, so it is straightforward to take into account the cascading process of de-excitation, which is important in determining the expected line intensities of low n transitions. With standard grazing-incidence VUV spectrometers, only a rather modest diagnostic neutral

hydrogen beam of perhaps 0.1 amperes is required, if the beam is modulated in time and phase-sensitive detection techniques are used. Figure 6 shows the modulation in 102Å OVII n = 3 → 2 prompt de-excitation radiation observed in PDX, using only a ~ 10 kW, 25 keV diagnostic neutral beam. The beam was square wave modulated at 500 Hz. By scanning the intersection point of the beam and spectrometer across the plasma, radial profiles of the density of fully stripped impurities can be obtained. Since recombination times are typically comparable to transport times for fully stripped low-Z impurities, one can expect to see large deviations from coronal equilibrium in these charge states. Figure 7 shows radial profiles of O^{+8} and C^{+6} measured on PDX using the charge exchange recombination technique /24/. The absolute impurity densities are consistent with Z_{eff} determined from the plasma resistivity and from the visible bremsstrahlung emission. The radial profiles are much broader than predicted by coronal equilibrium, but if a radially constant diffusion coefficient of order 10^4 cm^2/sec is used in an impurity transport code calculation /25/, then reasonable agreement with the data is found. This value for D is consistent with the value required to model impurity transport experiments in PDX based on pulsed impurity injection using the laser blow-off technique /26/.

Charge exchange recombination can be used for other purposes beyond impurity density measurements. Bright lines can be excited in the near UV by charge exchange recombination. These lines can then be used for Doppler shift and Doppler broadening measurement of plasma rotation /27/ and ion temperature. The use of a scanning system based on a modulated diagnostic neutral beam seems to promise the possiblility of a straightforward, reliable measurement of $T_i(r,t)$, and $V_\phi(r,t)$.

FAST ION DIAGNOSTICS

The diagnostic techniques described so far have depended exclusively on the interaction of an injected neutral atom beam with the charged particles in the plasma. When a collimated neutral beam is injected tangentially into a tokamak plasma, however, it is possible to create a local concentration of circulating fast ions within the plasma, and the interaction of these ions with the plasma particles and magnetic fields can be used for plasma diagnostics. If the beam is aimed at the magnetic axis, a centrally peaked distribution is created, assuming that the beam energy is high enough for good penetration, while if the beam is aimed at $R_0 + x$, a hollow ring of fast ions will be created at $r \approx x$.

Some preliminary experiments have been performed in an attempt to make use of measurements of the thermalization process of circulating energetic ions. The charge exchange spectrum from fast ions traveling in a tokamak plasma is sensitive to Z_{eff} through the pitch angle scattering rate, and to the neutral density profile, n_0, through the depletion of beam ions by charge exchange loss. Increased Z_{eff} results in increased signal at angles away from the injection angle, due to increased angular scattering, and increased neutral density results in a relative decrease in signal at lower energies, due to the loss of particles by charge exchange as they slow down. By using a collimated beam that injects tangentially outside of the magnetic axis, one can in principle measure profiles of n_0 and Z_{eff}. Figure 8 shows schematically the approach to measuring these profiles using a multi-angle charge exchange analyzer, and a collimated neutral beam. Preliminary experiments have been made on PDX using this technique /28,29,30/. Figure 9 shows a slowing down spectrum from PDX, with injection close to the magnetic axis. In this case theoretical calculations of the slowing down spectrum

/31,32/ based on the laser Thomson scattering electron temperature and density profiles give reasonable agreement with experiment, for Z_{eff} in the range of about 1.0 to 2.0. More detailed measurements, over a somewhat wider range in pitch angle, will be required in order to obtain a high degree of precision. In large tokamaks, n_0 is low enough in the core of the plasma that little depletion of the fast ion population is expected. This makes the spectra insensitive to n_0 in the central region.

More extensive measurements of $Z_{eff}(r)$ were made on the ATC tokamak /32/. Figure 10 summarizes the results. In standard discharges Z_{eff} was found to be somewhat peaked on axis and in relatively good agreement with the laser measurement based on the plasma resistivity. In a runaway discharge induced by using a significant fraction of neon in the fill gas, the laser measurement gave a low Z_{eff}, due to the nonthermal nature of the current carriers. The pitch angle scattering measurement, however, gave a result more consistent with the known large concentration of neon.

Another diagnostic technique which uses a localized circulating beam of fast ions was also developed on ATC /33/. This technique makes use of the shift of energetic ions from flux surfaces in order to measure q, the safety factor, inside of the plasma. The geometrical center of the orbit of a parallel moving ion is shifted from the center of the flux surfaces it is traveling on by a quantity $\Delta = qv/\Omega_{ci}$. Thus if one can accurately measure this orbit shift, one has a local, internal measurement of q. In practice it is difficult to determine the location of the magnetic surfaces accurately, so one measures the relative shift of orbits of particles with different momenta. A neutral beam emits H_0 neutrals at E_{inj}, $E_{inj}/2$ and $E_{inj}/3$, due to the breakup of H_2^+ and H_3^+ in the neutralizer. These evidently have different momenta, and different orbits, when they are captured in the plasma. In

addition a fraction of H_2^0 neutral molecules are emitted at E_{inj}, and at 2/3 E_{inj}, and some of these are captured in the plasma as H_2^+. They are detected by looking for H^0 dissociation products emerging from the plasma, rather than by using the usual resonant charge exchange process. These molecular ions have considerably greater momentum than the atomic ions. They are dissociated rapidly, however, and in high density plasmas are lost before they can be used for diagnostic purposes. At lower densities they permit a wider range of momenta, and therefore of orbit shifts, to be studied (Fig. 11).

In the ATC tokamak the orbit shifts were examined by moving the plasma in time, and looking at the evolution of the signal in one sight-line of a charge exchange analyzer. The injected beam was aimed outside of the magnetic axis, and the detector aimed to the inside of the magnetic axis. The beam was square wave modulated at 3 kHz in order to help discriminate against particles which had circulated in the plasma for long enough to begin to pitch angle scatter. Thus the appearance of modulated flux at the analyzer indicated that the plasma had been moved to the correct position such that the analyzer was looking at the opposite (inside in major radius) edge of the orbit surface of the freshly injected ions. A slightly different plasma position was required for each particle momentum, reflecting the different orbit shifts. Figure 12 shows the measured orbit shifts for a typical example in ATC. Note that the displacement is measured by the plasma major radius required for maximum modulated flux.

On PDX it was deemed impractical to move the plasma in time for this measurement. Therefore a new type of spatially imaging neutral particle detector was developed /28/. This detector has a pinhole camera type of input geometry in the horizontal plane, followed by a fan geometry stripping cell, which preserves the spatial information of the "camera." Ions emerging from

the stripping cell are deflected in the vertical direction by a 127° cylindrical plate electrostatic energy analyzer, and focussed on a large area micro channel-plate (MCP) array. The MCP array has a multi-anode particle collector, whose output goes to an array of amplifiers, giving spatially resolved measurements of the charge exchange signal. The total system has $\lesssim$ 1 cm spatial resolution, 3% energy resolution, and down to 10 micro-second time resolution, in its present configuration.

Figure 13 shows a spatially resolved measurement of the inner edge of an orbit drift surface in PDX. "Major radius" in this figure indicates R_{tan}, the distance of closest approach of the sight-line to the vertical axis of symmetry of the tokamak. The magnetic axis is off to the right, and the modulated neutral beam was injected outside of the magnetic axis. Note the sharp cut-off in signal as the detector looks inside (in minor radius) of the hollow ring of fast ions. This is because fast ions can only be seen at this location due to anomalous spatial diffusion, which is evidently not significant.

Because the plasma is stationary in the PDX measurements, the time evolution of q can be measured during a long ($\lesssim$ 40 msec) beam pulse. Some preliminary measurements of q(0) during sawtooth oscillations, for example, give δq = 0.2 at each internal disruption. During the initial current penetration phase, rather dramatic signals are seen as the modulated circulating ion beam is swept across the detector sight-lines by the changing internal poloidal flux. Figure 14 shows the time evolution of the signal at two tangency radii during current penetration. These data are from the same case as Fig. 13. In that figure, the orbit surface inner edge was located at about 105 cm at t = 50 msec. Clearly it moved significantly during the 15 msec period shown in these figures. (Note that in these cases the diagnostic

neutral beam was injecting in the counter direction, so the orbits move outwards in major radius as the poloidal flux increases.) The full time evolution of q near the plasma center is shown in Fig. 15. The central q value decreases smoothly as the edge q falls, and then it continues to fall as the plasma current is held constant. Comparisons of these results with magnetic diffusion calculations are now being made. The central q's measured in ATC during steady state with this technique disagreed significantly with those deduced from Thomson scattering measurements. In general the laser measurement, assuming either Spitzer or neoclassical resistivity, gave a central q much lower than the orbit measurement, and below 1 even in cases without sawtooth oscillations. The centrally peaked Z_{eff} measured in ATC gives a reasonable explanation for this discrepancy.

FLUCTUATION MEASUREMENTS

In the previous section we discussed the use of classical beam ion thermalization and orbit shifts for plasma diagnostics. In strongly MHD dominated discharges, charge-exchange signals during neutral beam injection show significant effects due to the instabilities. As early as on ATC the tangential charge-exchange flux from the circulating heating beam ions was seen to show oscillations at the same frequency as strong m = 2 oscillations seen on the Mirnov coils. This same effect has been seen on PDX in m = 2 dominated discharges. However in the absence of supporting measurements one cannot tell whether this is due to a fluctuating neutral density, changes in the flux surface shapes, or motion of the beam ions relative to the bulk plasma. Slowing down measurements on PDX show no significant depletion of the fast ion spectrum below E_{inj} due to these oscillations. A particularly interesting experiment was performed by injecting the PDX horizontal

collimated diagnostic neutral beam into an m = 2 dominated plasma (Fig. 16). The beam was injected at a tangency radius of 147.6 cm. The two detector channels closest to the injection angle were at 140.2 and 151.8 cm. The plasma center was at 135 cm, and the detector energy analyzer was set to look near E_{inj}. A very strong modulation was seen in the detector signals during injection from 205 to 215 msec. However the beam was not modulated in this case. Rather the spatial motion of the flux surfaces carried the circulating fast ions back and forth across the detector sight-line. Note that the oscillations are out of phase in the two channels, since they are on opposite sides of the injection angle. From the known shape of the diagnostic neutral beam, one can deduce that the plasma motion must have been on the order of 5 cm to cause this degree of oscillation. More detailed measurements, with the detector array arranged in a configuration to give the motion of the beam peak directly, are clearly called for.

New MHD oscillations called "fishbones" are observed on PDX during high power neutral beam injection at low toroidal fields /34/. These oscillations cause spikes of perpendicular charge exchange flux to be emitted from the plasma, and after each spike the high energy portion of the beam ion distribution function is depleted (Fig. 17). Each spike is composed of a large number of individual particle bursts (not seen here) which are frequency and phase locked to the 5 - 20 kHz Mirnov signals.

Measurements of the parallel thermal ion distribution function during sawtooth and intense fishbone oscillations have been made, using one of the PDX heating beams for local doping (Fig. 18). The tangential view that is obtained across the perpendicular heating beam gives very good spatial localization, and such strong local doping that ~ 90% of the signal seen is due to the presence of the heating beam. Under these circumstances behavior

very similar to that seen in the electrons by the X-ray diode array is seen in the parallel thermal ion distribution function. Sawteeth and sawtooth precursor oscillations are observed (Fig. 19), and the sawtooth inversion radius is found to lie at about t same location as determined from the X-ray diagnostic. A surprising fact is that in low q discharges the fast inverted sawtooth is found at the plasma edge within about 150 micro-seconds of the time it is seen at the q = 1 surface /35/. During this time the 5 - 10 keV parallel moving ions can only make $\lesssim$ 30 transits around the machine. This result does not seem consistent with theories which ascribe the sawtooth behaviour to field line ergodicity, rather than to reconnection. During moderate fishbone activity, parallel ion sawteeth are not observed at each fishbone. But at very low fields and high powers, each fishbone oscillation is seen to cause a jump down in the central parallel ion distribution, and an increase at the edge, very similar to a normal sawtooth, only more frequent.

CONCLUSIONS

We have described here a number of plasma diagnostic techniques which rely on the use of hydrogen neutral beams. Some of these techniques, such as beam attenuation measurements, have been used since the beginning of research in fusion plasma physics. Others, such as charge exchange recombination, are very new and show great promise. Still others, such as active charge exchange, have begun to become standard techniques and yet their potential has not been completely explored. It seems that the wisest conclusion to draw from all of this is that plasma physics experimenters are constantly in search of new diagnostic techniques and are constantly remolding the old methods. In this context a hydrogen neutral beam, which interacts with an ionized gas in so many ways, is an ideal building block, and what we experimenters will build with it in the future can hardly be imagined at this time.

ACKNOWLEDGMENTS

The author would like to acknowledge the skillful collaboration of Dr. R. Kaita, D.D. Meyerhofer, and D.L. Herndon in the PDX fast ion diagnostic experiments. This work was supported by the U.S. Department of Energy Contract No. DE-AC02-76-CHO-3073.

REFERENCES

1. H. Eubank, P. Noll, F. Tappert, Nucl. Fusion 5 (1965) 58.
2. R.L. Freeman, E.M. Jones, Culham Laboratory Report CLM-R137 (1974).
3. R.E. Olson et al., Phys. Rev. Letters 41 (1978) 163.
4. M.A. Heald, C.B. Wharton, Plasma Diagnostics with Microwaves, Wiley, New York (1965).
5. W.C. Turner et al., Nucl. Fusion 19 (1979) 1011.
6. Equipe TFR, Nucl. Fusion 19 (1979) 1261.
7. D.F. Düchs, D.E. Post, P.H. Rutherford, Nucl. Fusion 17 (1977) 565.
8. G.H. Neilson, Oak Ridge National Laboratory Report (1979) ORNL/TM-6823.
9. V.V. Afrosimov, M.P. Petrov, V.A. Sadovnikov, JETP Letters 18 (1973) 300.
10. A.M. Kudryavtsev, A.F. Sorokin, JETP Letters 16 (1973) 286.
11. H.P. Eubank, in Course on Plasma Diagnostics and Data Acquisition, Ed. H. Eubank, E. Sindoni, C.N.R. Euratom (1975) 152.
12. S.L. Davis, D. Mueller, C. Keane (to be published).
13. S.S. Medley, R.J. Goldston, H.H. Towner, Princeton Plasma Physics Laboratory Report (1980) PPPL-1673.
14. H.H. Towner, R.J. Goldston in Bull. Am. Phys. Soc. 24 (1979) 1107.
15. E.S. Marmar et al., in Bull. Am. Phys. Soc. 25 (1980) 951.
16. R.E. Olson, A. Salop, Phys. Rev. A 16 (1977) 531.
17. H. Ryufuku, T. Watanabe, Phys. Rev. A. 18 (1978) 2005.
18. A Salop, J. Phys. B: Atom. Molec. Phys. 12 (1979) 919.
19. T.A. Green, E.J. Shipsey, J.C. Browne, Phys. Rev. A 23 (1981) 546.
20. R.E. Olson, Phys. Rev. A 24 (1981) 1726.
21. R.C. Isler et al., Phys. Rev. A 24 (1981) 2701.
22. V.V. Afrosimov et al., Sov. J. Plasma Physics 5 (1979) 551.

23. A.N. Zimovev et al., JETP Letters 32 (1980) 539.

24. R.J. Fonck et al., Phys. Rev. Lett. 49 (1982) 737.

25. R.A. Hulse, to be published in Nucl. Tech./Fusion.

26. R.A. Hulse et al., in Bull. Am. Phys. Soc. 26 (1981) 864.

27. R.C. Isler, private communication (1982).

28. R. Kaita et al., Rev. Sci. Instrum. 52 (1981) 1795.

29. A. Nudelman, R. Goldston, R. Kaita, J. Vac. Sci. and Technol. 30 (1982) 1218.

30. D.D. Meyerhofer et al., in Bull. Am. Phys. Soc. (1982) 6Q4, to be published.

31. R.J. Goldston, Nucl. Fusion 15 (1975) 651.

32. R.J. Goldston, Ph.D. Dissertation, Princeton University (1977).

33. R.J. Goldston, Phys. Fluids 21 (1978) 2346.

34. D.L. Johnson et al., in Plasma Physics and Controlled Nuclear Fusion Research 1982, Vol. 1, to be published.

35. H.P. Eubank et al., in Proceedings of Third Joint Varenna-Grenoble International Conference on Heating in Torodial Plasmas, to be published.

FIGURE CAPTIONS

Fig. 1 Diagram showing neutral penetration into a tokamak plasma. Multi-generation wall source neutrals, primary beam neutrals, and beam halo neutrals all contribute to the target for charge exchange.

Fig. 2 (a) Passive and (b) active charge exchange spectra from PLT with high power neutral beam injection.

Fig. 3 Charge-exchange signals from a ten channel neutral particle analyzer on PDX. Diagnostic neutral beam is on steadily for 15 msec during an ohmic discharge.

Fig. 4 Configuration of the TFTR vertical charge exchange system, including a horizontal diagnostic neutral beam.

Fig. 5 Illustration of the contribution of halo doping neutrals to the modulation in neutral particle flux for the TFTR vertical charge-exchange system. Line types indicate particular analyzers, as shown in Fig. 4.

Fig. 6 Modulated O VIII 102 Å ($n = 3 \rightarrow 2$) emission due to charge exchange with the modulated diagnostic neutral beam.

Fig. 7 Radial profiles of fully ionized oxygen and carbon during the steady-state phase of a PDX discharge. Limiter radius is at $r = 30$ cm; $R_o = 147$ cm. Closed circles: $R > R_o$. Open circles: $R < R_o$.

The solid lines are radial profiles of C^{6+} and O^{8+} calculated from impurity transport code. C.E. = distribution expected from coronal equilibrium assuming a constant impurity density. D = constant impurity diffusion coefficient.

Fig. 8 Schematic diagram of beam and detector aiming to measure Z_{eff} on axis, and then further out in minor radius in a tokamak.

Fig. 9 Slowing down measurement for diagnostic neutral beam aimed near $R = R_o$ on PDX.

Fig. 10 2 to 3 point Z_{eff} "profiles" from ATC, measured by the scattering rate of fast ions.

Fig. 11 Illustration of orbit shifts for co-injected ions with various momenta.

Fig. 12 Measured orbit shifts on ATC corresponding to q(o) = 1.0. The orbit widths were great enough here that dq/dr had to be taken into account. Thus the orbit shift data are fit with a curved line.

Fig. 13 Measured shape of the circulating ion beam at t = 47-53 msec during PDX start-up, using multi-sight-line charge exchange analyzer.

Fig. 14 (a) Time variation of neutral particle flux for sight-line aimed at R_{tan} = 99 cm. Same conditions as Fig. 13 (Beam modulated at 1 KHz). (b) Time modulated neutral particle flux for sight-line aimed at R_{tan} = 107.5 cm.

Fig. 15 Time evolution of q(a) and q measured near the plasma center for PDX start-up.

Fig. 16 Modulated neutral flux from circulating diagnostic neutral beam ions, due to m=2 instability. Beam is on continuously from t = 205 to 216 msec.

Fig. 17 Modulation in 40 keV perpendicular neutral particle flux due to "fishbone" instability. Each spike corresponds to a fishbone seen on the Mirnov coils, and faster time resolution reveals a fast (8-20 kHz) internal modulation of the enhanced signal, phase-locked to the Mirnov signals /34/. After each spike the charge-exchange spectrum at high energies is depleted, and then is filled in by particles slowing down from $E_{inj} \simeq 47$ keV.

Fig. 18 Diagram showing doping due to PDX Northwest beamline for fast ion diagnostic experiment multi-sight-line charge-exchange detector oriented to view parallel moving ions. Detector can view to $R_{tan} = R_o+a$. Doping due to NW beam generally increases signal level by a factor of $\sim$ 10, making fast local measurements of $f_{i\parallel}$ possible.

Fig. 19 Observation of sawtooth precursor oscillation and sawtooth on $f_{i\parallel}$ using geometry of Fig. 18.

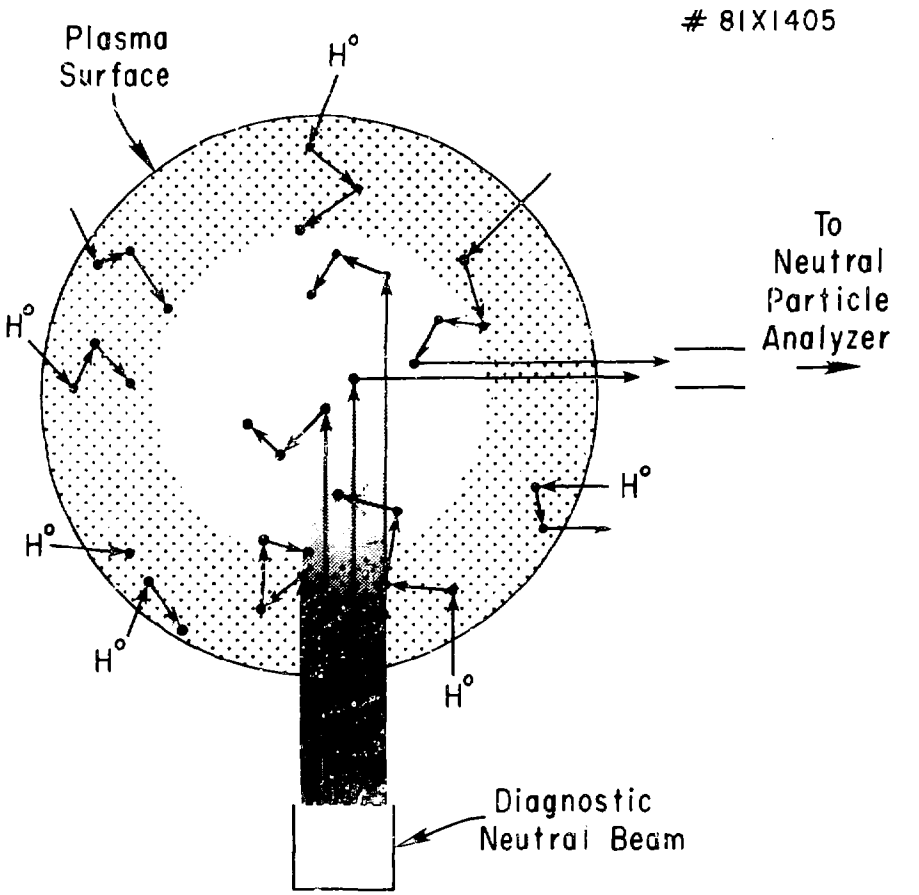

$$H^{\circ}_{slow} + H^{+}_{fast} \rightarrow H^{+}_{slow} + H^{\circ}_{fast}$$

$$H^{\circ} + e^{-} \rightarrow H^{+} + 2e^{-}$$

Fig. 1

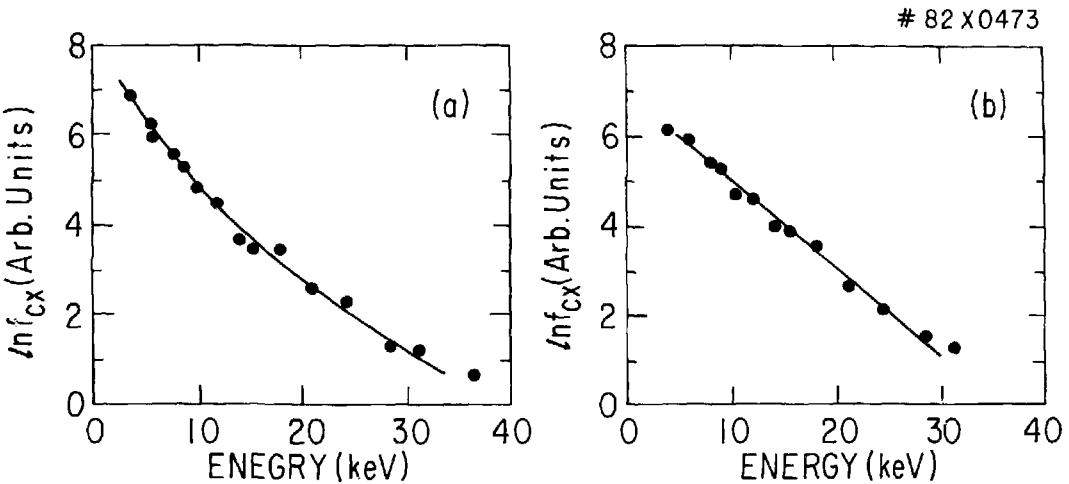

Fig. 2

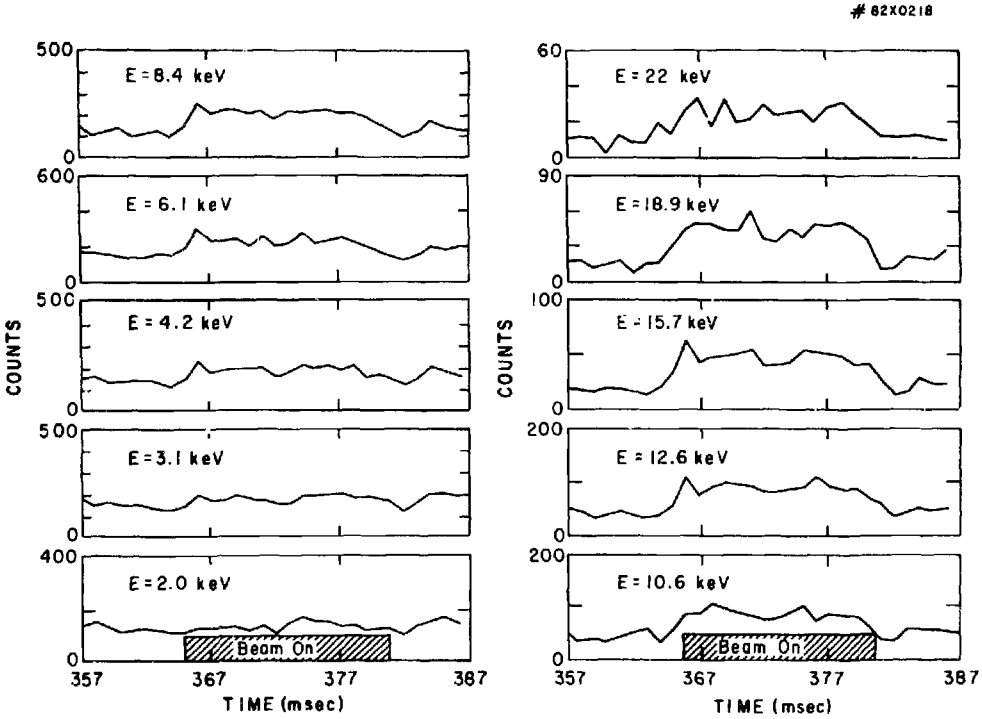
#82X0218
E = 8.4 keV
E = 6.1 keV
E = 4.2 keV
E = 3.1 keV
E = 2.0 keV
E = 22 keV
E = 18.9 keV
E = 15.7 keV
E = 12.6 keV
E = 10.6 keV
Beam On
COUNTS
TIME (msec)
357
367
377
387

Fig. 3

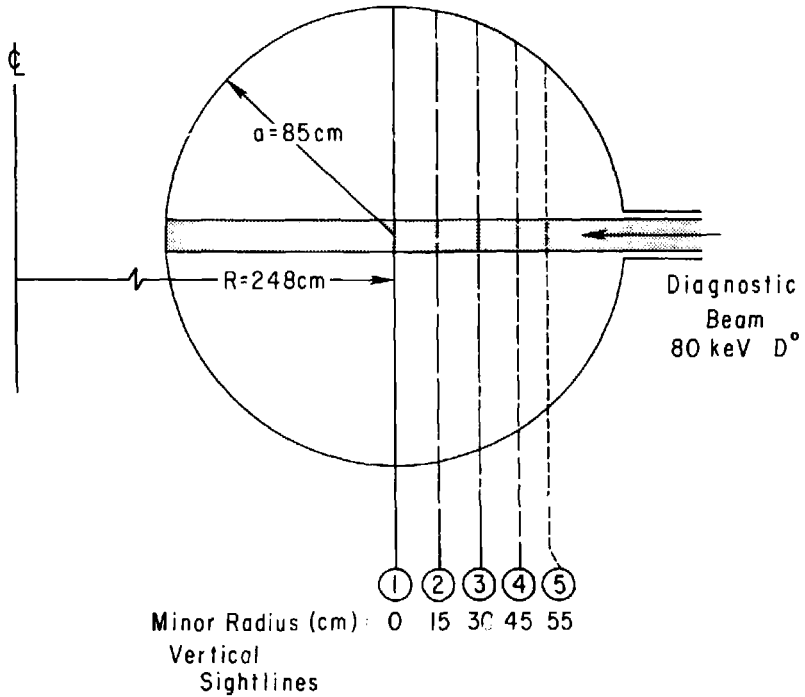
℄
a=85cm
R=248cm
Diagnostic
Beam
80 keV D°
1 2 3 4 5
Minor Radius (cm) 0 15 30 45 55
Vertical
Sightlines

Fig. 4

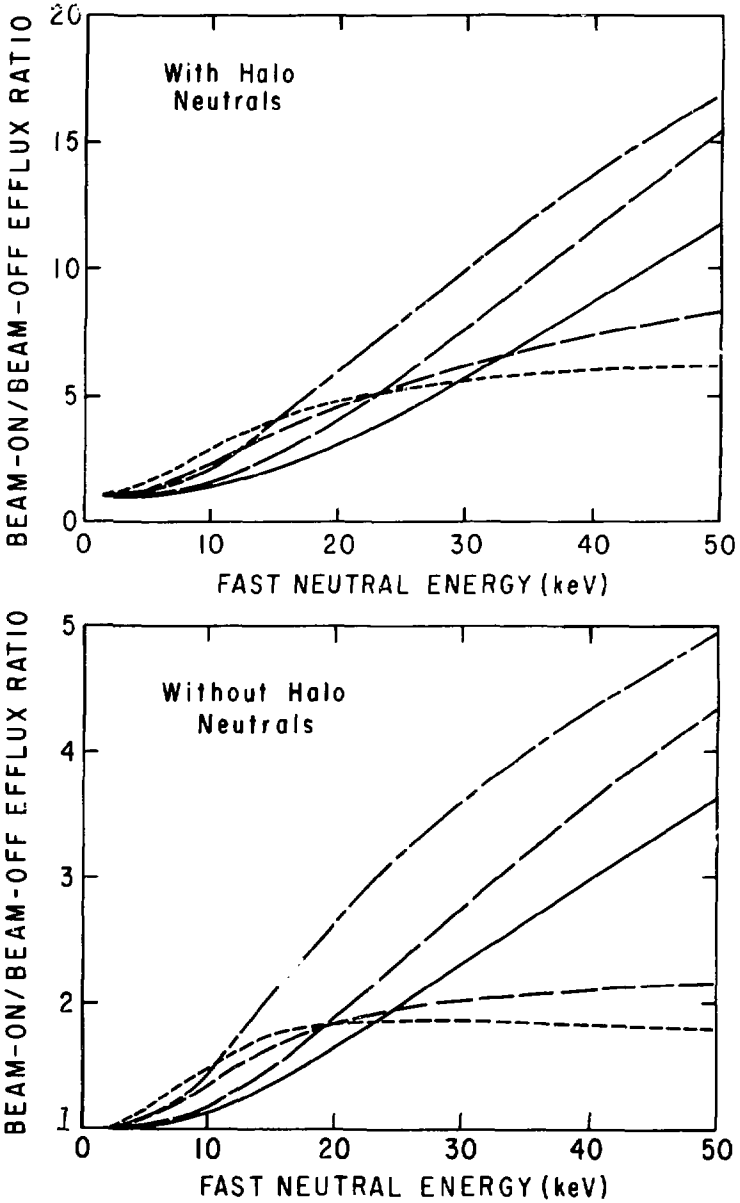
With Halo Neutrals
BEAM-ON/BEAM-OFF EFFLUX RATIO
FAST NEUTRAL ENERGY (keV)
Without Halo Neutrals
BEAM-ON/BEAM-OFF EFFLUX RATIO
FAST NEUTRAL ENERGY (keV)

Fig. 5

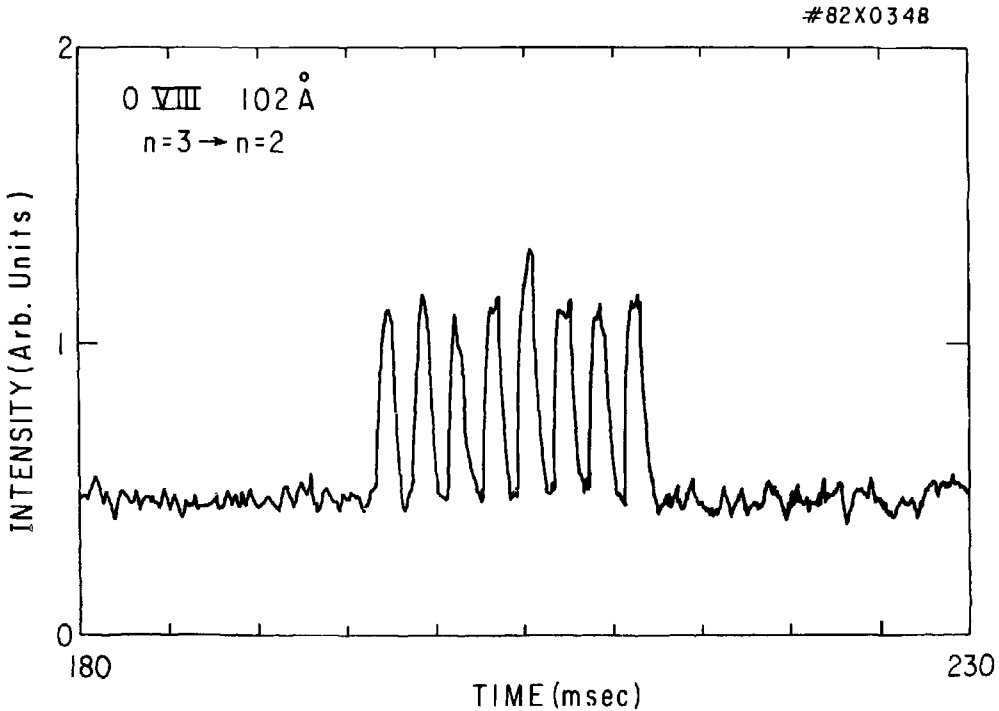
#82X0348
O VIII 102 Å
n=3 → n=2
INTENSITY (Arb. Units)
2
1
0
180
230
TIME (msec)

Fig. 6

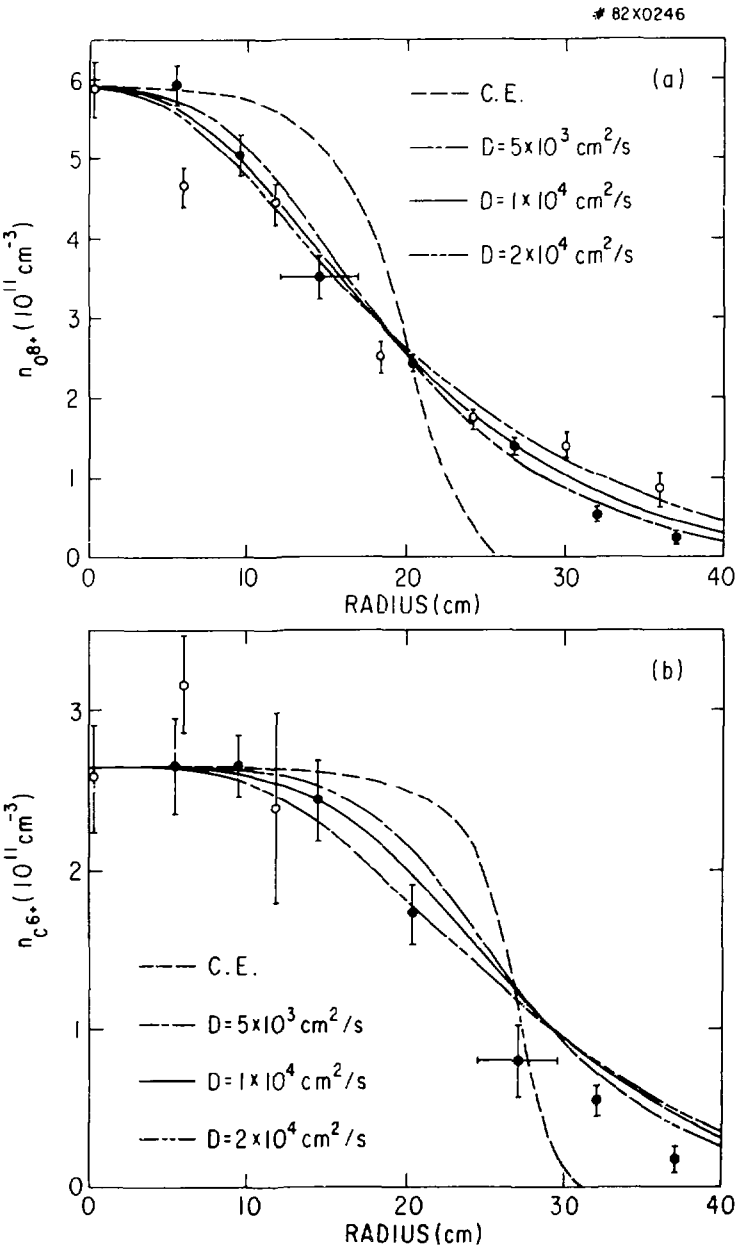
#82X0246
(a)
C.E.
D=5x10^3 cm^2/s
D=1x10^4 cm^2/s
D=2x10^4 cm^2/s
n_O8+ (10^11 cm^-3)
RADIUS (cm)
(b)
C.E.
D=5x10^3 cm^2/s
D=1x10^4 cm^2/s
D=2x10^4 cm^2/s
n_C6+ (10^11 cm^-3)
RADIUS (cm)

Fig. 7

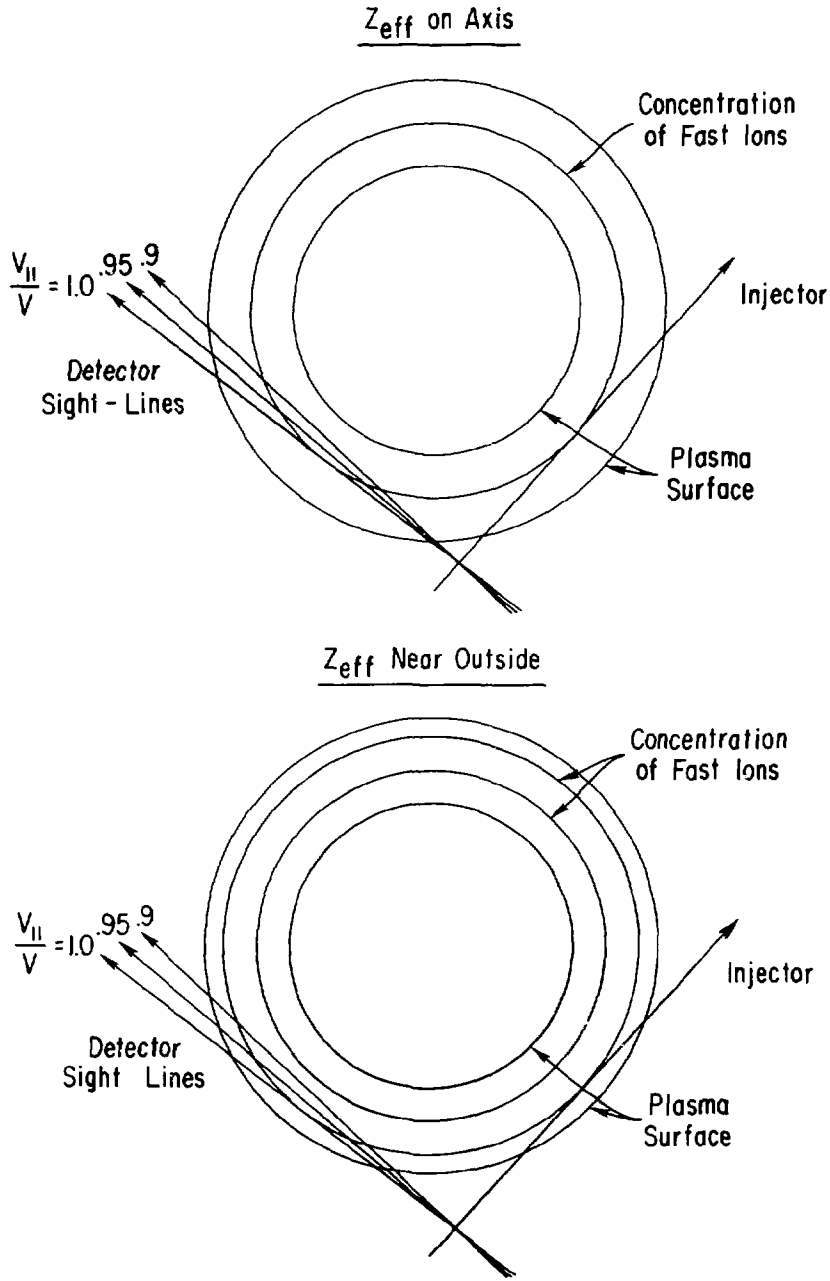
Z_{eff} on Axis
Concentration of Fast Ions
$\frac{V_{||}}{V}$ = 1.0 .95 .9
Injector
Detector Sight - Lines
Plasma Surface
Z_{eff} Near Outside
Concentration of Fast Ions
$\frac{V_{||}}{V}$ = 1.0 .95 .9
Injector
Detector Sight Lines
Plasma Surface

Fig. 8

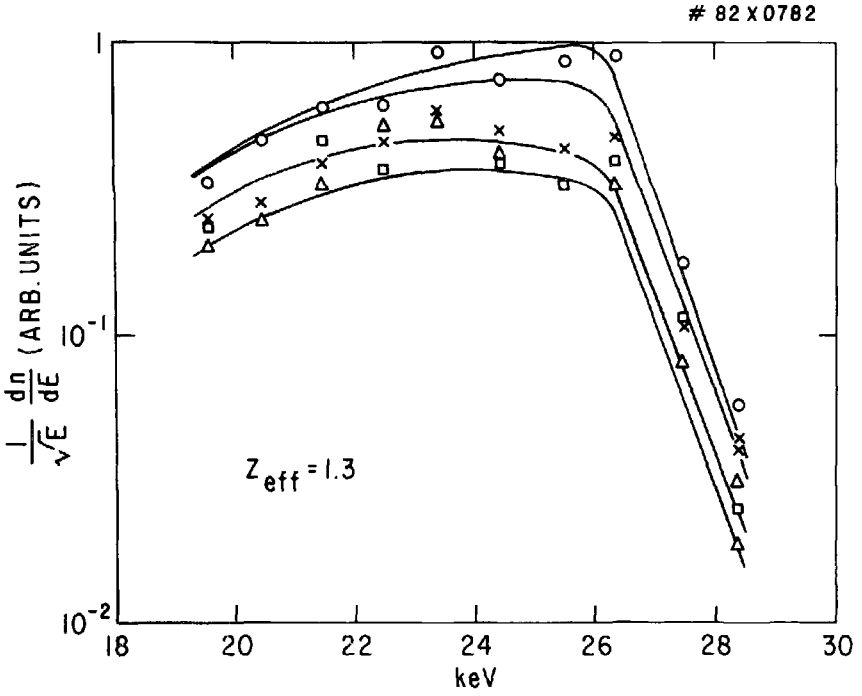
82 X 0782
1
10^{-1}
10^{-2}
$\frac{1}{\sqrt{E}} \frac{dn}{dE}$ (ARB. UNITS)
$Z_{eff} = 1.3$
18
20
22
24
26
28
30
keV

Fig. 9

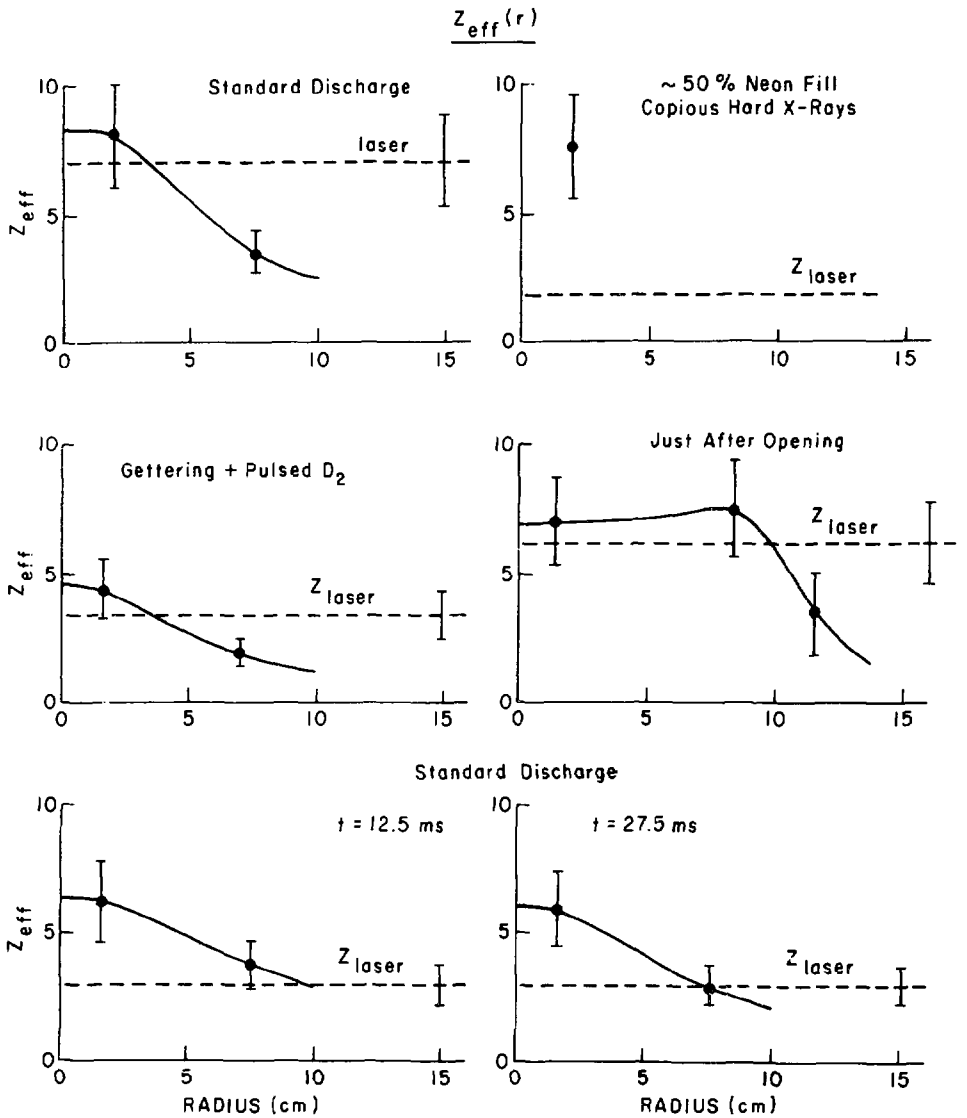
$Z_{eff}(r)$
Standard Discharge
laser
~ 50 % Neon Fill
Copious Hard X-Rays
Z_{laser}
Gettering + Pulsed D_2
Z_{laser}
Just After Opening
Z_{laser}
Standard Discharge
t = 12.5 ms
Z_{laser}
t = 27.5 ms
Z_{laser}
Z_{eff}
RADIUS (cm)
RADIUS (cm)

Fig. 10

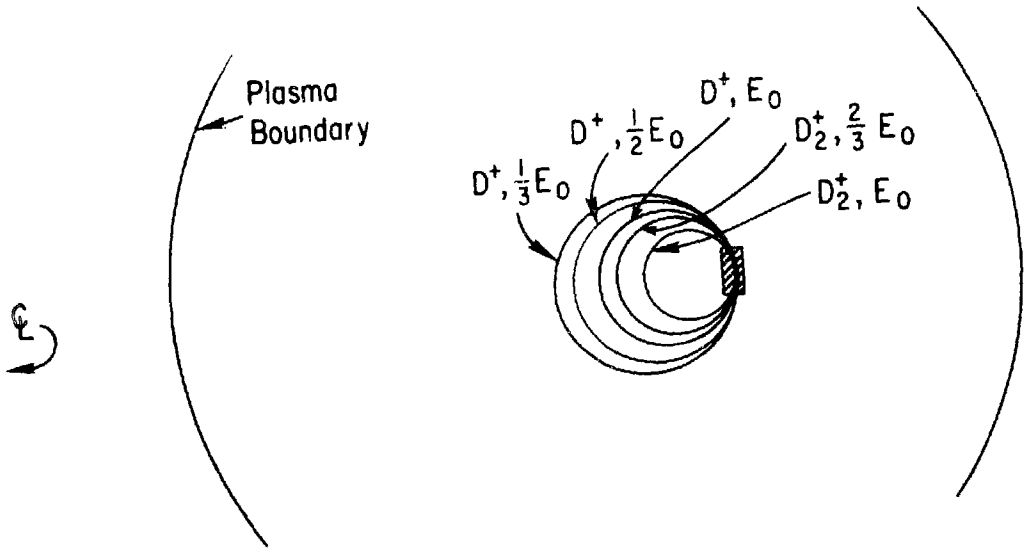

Fig. 11

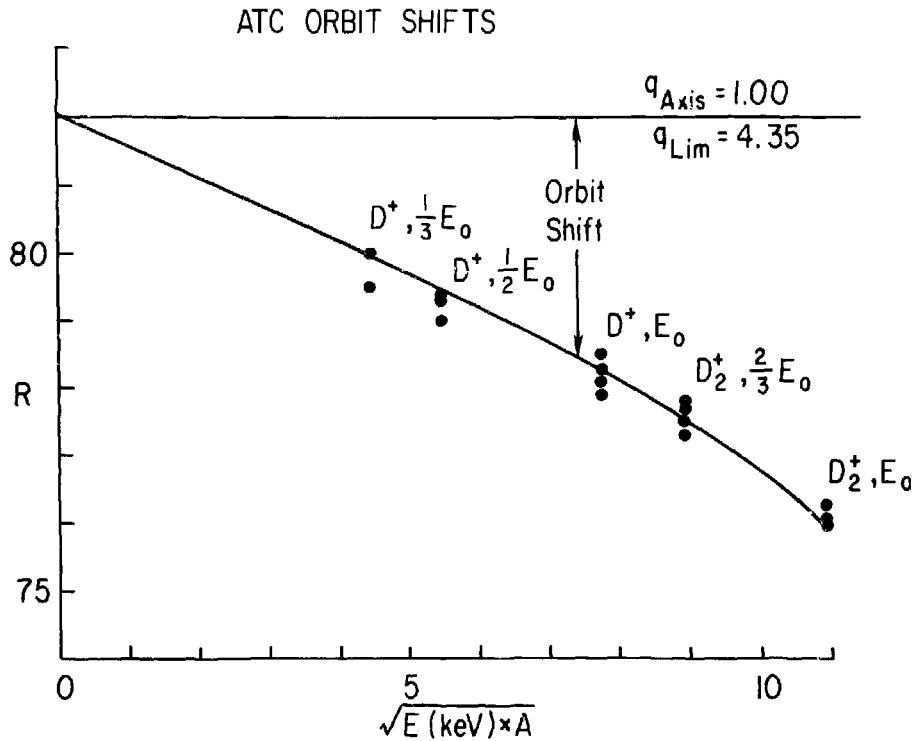
ATC ORBIT SHIFTS
$q_{Axis} = 1.00$
$q_{Lim} = 4.35$
Orbit Shift
$D^+, \frac{1}{3}E_o$
$D^+, \frac{1}{2}E_o$
D^+, E_o
$D_2^+, \frac{2}{3}E_o$
D_2^+, E_o
80
R
75
0
5
10
$\sqrt{E\,(keV) \times A}$

Fig. 12

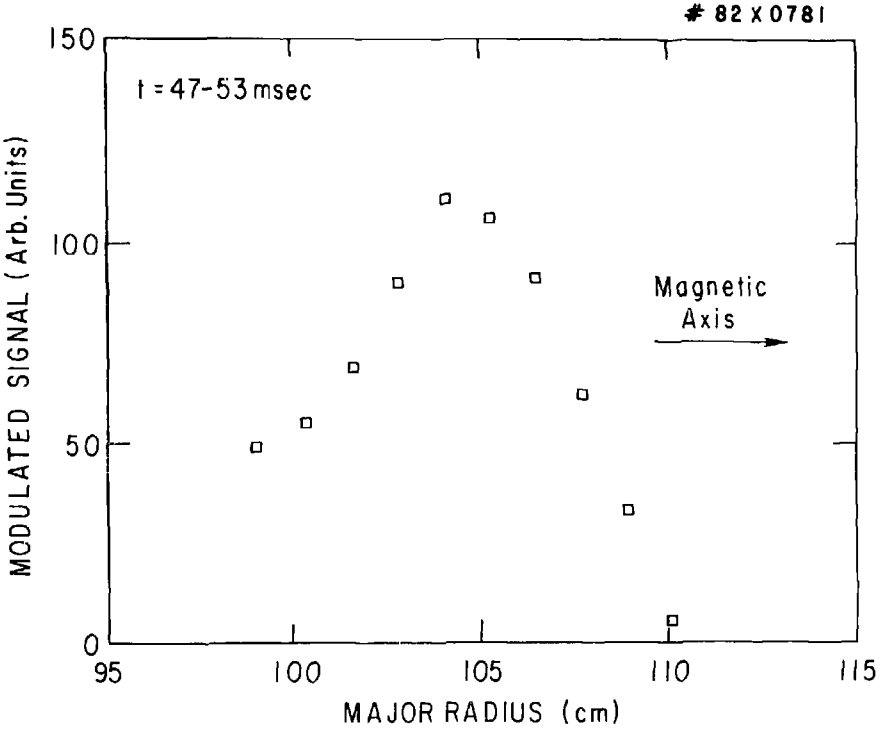
82 X 0781
150
100
50
0
t = 47-53 msec
Magnetic
Axis
MODULATED SIGNAL (Arb. Units)
95
100
105
110
115
MAJOR RADIUS (cm)

Fig. 13

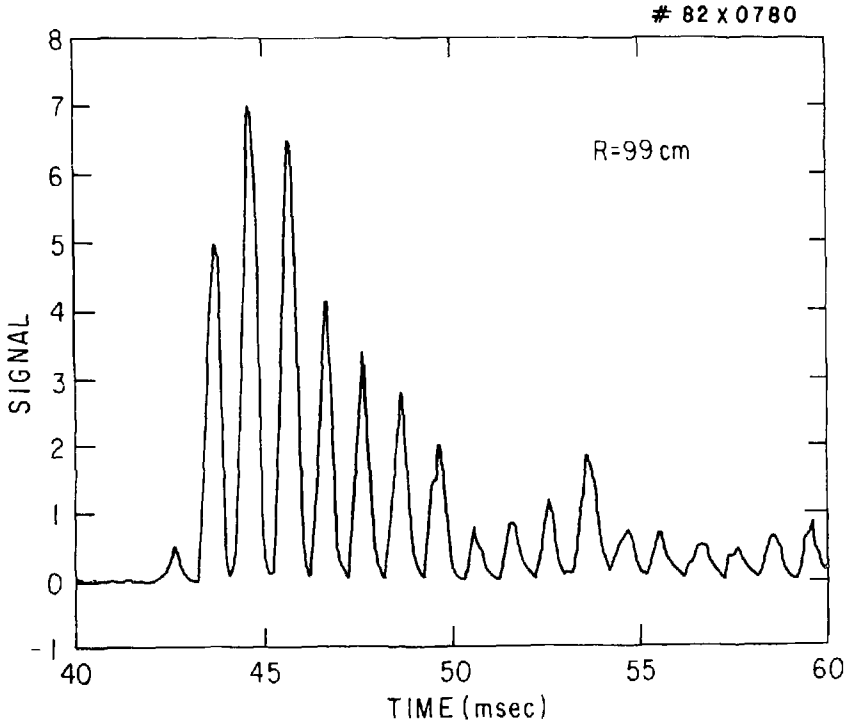

Fig. 14a

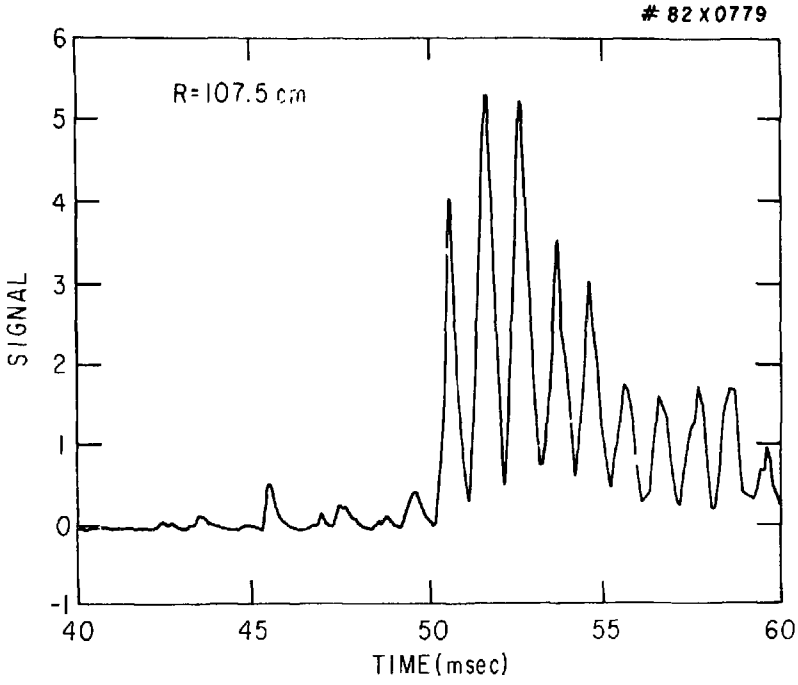

Fig. 14b

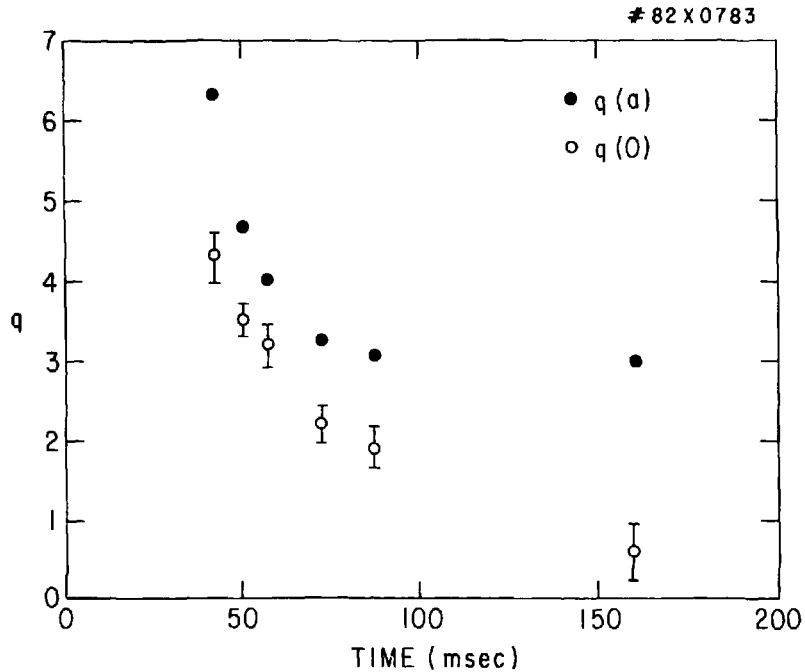

Fig. 15

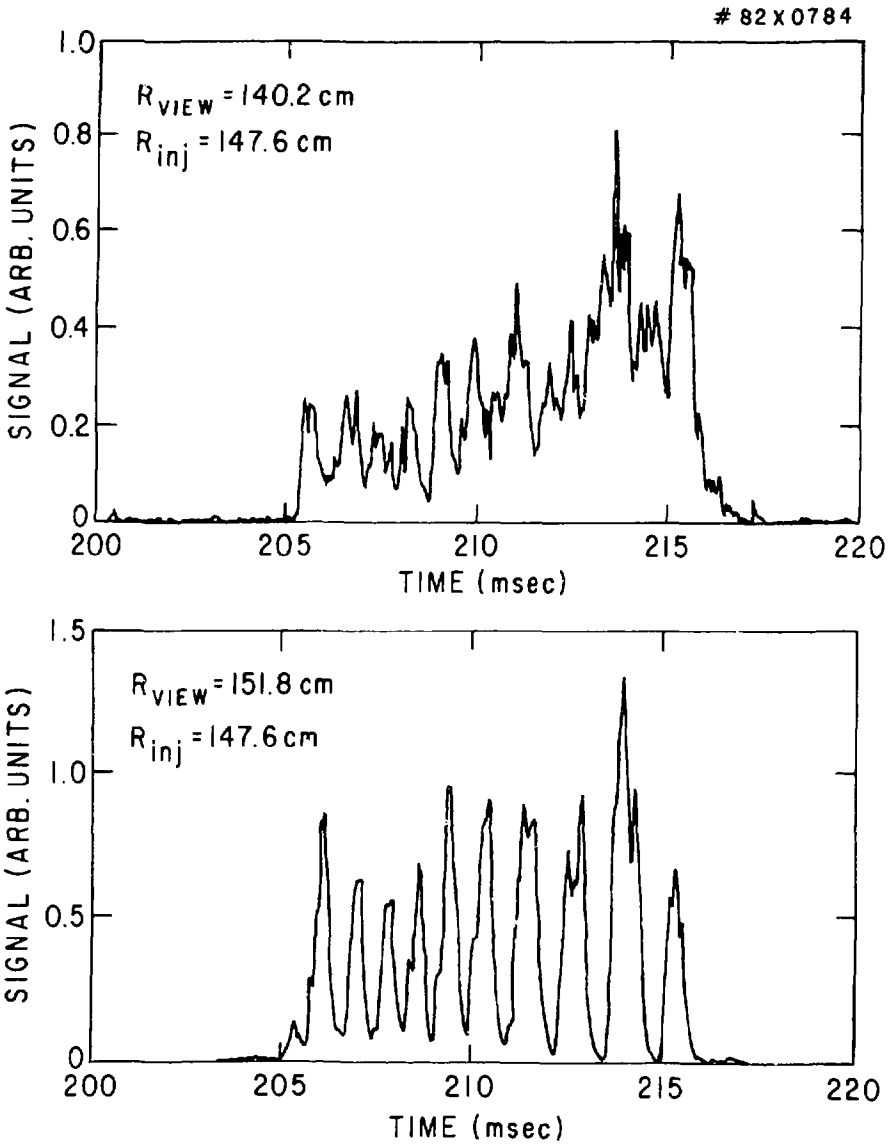
82X0784
R_{VIEW} = 140.2 cm
R_{inj} = 147.6 cm
SIGNAL (ARB. UNITS)
1.0
0.8
0.6
0.4
0.2
0
200
205
210
215
220
TIME (msec)
R_{VIEW} = 151.8 cm
R_{inj} = 147.6 cm
SIGNAL (ARB. UNITS)
1.5
1.0
0.5
0
200
205
210
215
220
TIME (msec)

Fig. 16

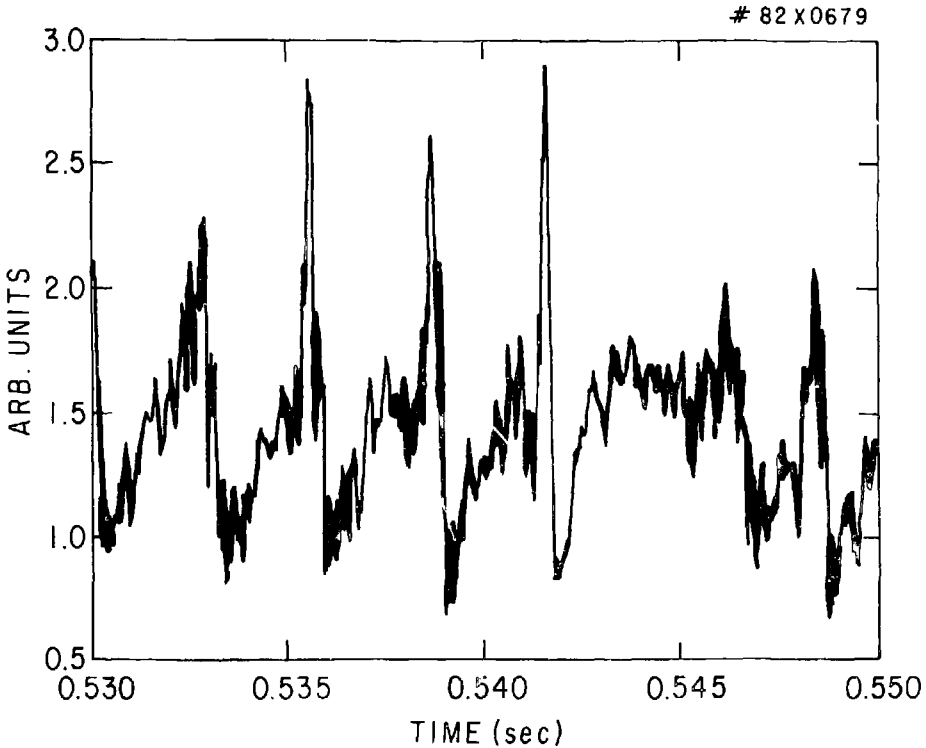
82 X 0679
3.0
2.5
2.0
1.5
1.0
0.5
ARB. UNITS
0.530
0.535
0.540
0.545
0.550
TIME (sec)

Fig. 17

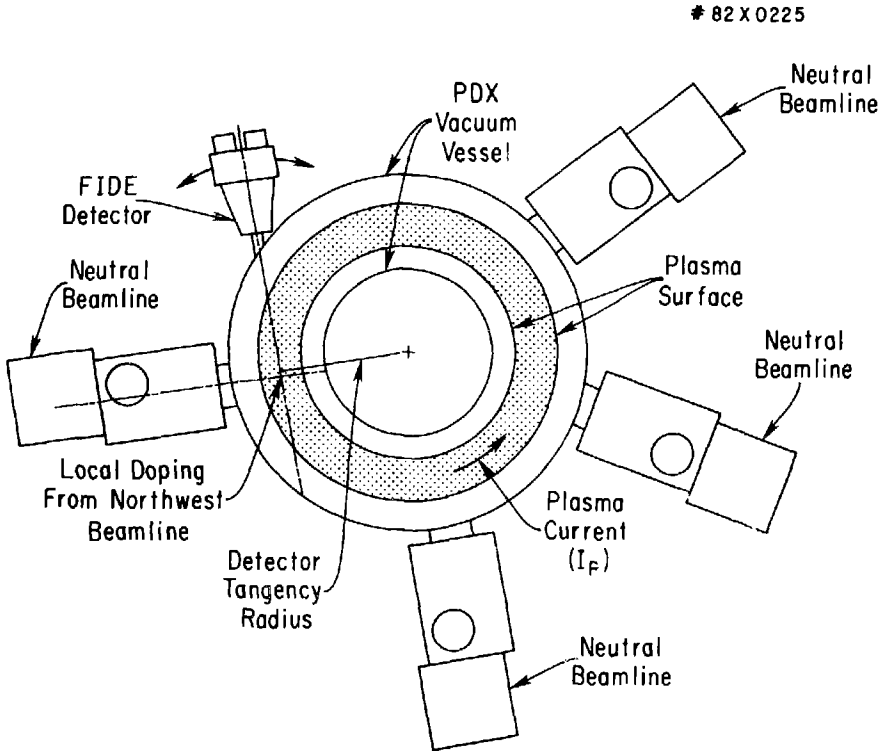
#82X0225
PDX
Vacuum
Vessel
Neutral
Beamline
FIDE
Detector
Neutral
Beamline
Plasma
Surface
Neutral
Beamline
Local Doping
From Northwest
Beamline
Plasma
Current
(I_P)
Detector
Tangency
Radius
Neutral
Beamline

Fig. 18

#81X1272